Generalized likelihood ratio-based condition indicator maximization via Rayleigh quotient iteration

K Kestel, C Peeters, Jérôme Antoni, Quentin Leclere, F Girardin, R Brijder, J Helsen

Generalized likelihood ratio-based condition indicator maximization via Rayleigh quotient iteration

K. Kestel [1,2], **C. Peeters** [1], **J. Antoni** [2], **Q. Léclere** [2], **F. Girardin** [2], **R. Brijder** [3], **J. Helsen** [1]
[1] Vrije Universiteit Brussel - VUB, Department of Applied Mechanics,
Elsene, Brussels, 1050, Belgium

[2] Univ Lyon, INSA Lyon, LVA,
EA677, 69621 Villeurbanne, France

[3] Flanders Make, Corelab DecisionS,
3920 Lommel, Belgium

Abstract
This study attempts to improve the performance of Generalized Likelihood Ratio Test-based indicators via blind filtering the of vibration signals. The key point is the optimization of the filter coefficients to maximize the indicator of interest. The filter coefficients are optimized through Rayleigh quotient iteration. The proposed method's performance and applicability are demonstrated on both simulated and real vibration signals measured on an experimental test rig. The outcome of the study shows that the Rayleigh quotient iteration is a potent tool for maximizing such complex condition monitoring indicators. Inspections over the filtered signals reveal that the optimal filters promote particular signal patterns linked to a bearing fault in vibration signals. The indicator estimated over the filtered signals is able to detect the bearing fault more robustly when compared to the raw signals.

1 Introduction

The tools to detect anomalies in rotating machinery based on vibration signals rapidly develop as the complexity of the machines increases. Modern rotating machines are comprised of an immense amount of components; therefore, tracking their health condition is a challenging task. Thanks to the ever-increasing computational power, we can now utilize reliable condition indicators (CI), which are computationally expensive. The potential of blind filtering for enhancing the fault detection capability of a complex condition monitoring indicator is investigated. The coefficients of the blind filter are optimized through the generalized Rayleigh quotient iteration. The proposed approach's performance is tested on both simulated and experimental vibration signals.

An early filter optimization approach to promote a signal's statistical feature is called the Minimum Entropy Deconvolution (MED) [1]. It was first introduced to recover the impulsive pattern in seismic signals by optimizing a filter that maximizes the kurtosis of the vibration signals. Approaches similar to MED with higher orders than fourth-order moments of a signal are studied further [2]. Nevertheless, kurtosis and its higher-order counterparts suffer from being sensitive to outliers that may occur due to strong noise. In order to benefit from the repetition of the impulses, for instance, emitted by a roller element bearing fault, Maximum Correlated Kurtosis Deconvolution (MCKD) is proposed as a part of the family of MED-based approaches [3]. Methods optimizing a filter while maximizing the feature of interest are not limited to kurtosis. Influenced by MED, a blind deconvolution method based on the Jarque-Bera statistic is also proposed [4]. Moreover, a novel application embedding the l_0-norm into the MED method has been introduced in literature [5] and shown to have the potential to overcome the shortcomings of the MED.

The common trend in vibration-based condition monitoring is toward using the second-order cyclostationary content within the signal, similar to MCKD. For example, rolling element bearing faults generate impulses which demonstrate the second-order cyclostationary pattern in vibration signals. In a recent study, a measure that quantifies the cyclostationary content embedded in vibration signals is maximized using a deconvolution filter which is optimized through Rayleigh quotient iteration [6]. The Rayleigh quotient iteration is also proposed to be used to maximize the sparsity of the envelope spectra for roller element bearing fault detection [7]. Likewise, several members of Box-Cox sparsity measures are used as the indicator of interest to optimize filters via the Rayleigh quotient [8]. The studies mentioned above summarize the key approaches in the literature that are developed to promote a feature in vibration signals by filtering them with optimal filters.

In this study, a novel CI based on the Generalized Likelihood Ratio Test (GLRT) [9] is utilized as the figure of merit to optimize the filter. Antoni and Borghesani devised several GLRT-based condition monitoring indicators to detect distinct fault-related patterns in vibration signals [9]. One of these indicators estimates the deviation of signal's distribution from the Gaussian for fault detection. In practice, the deviation from the Gaussian generally manifests itself as impulsiveness in vibration signals. This indicator is utilized as the measure to be maximized in the Rayleigh quotient optimization to estimate the optimal filter coefficients. The goal is to estimate the indicator on the filtered signals for early and robust detection of roller element bearing fault from vibration signals. The proof of concept is firstly performed on simulated signals; furthermore, performance tests are made on experimental vibration signals measured on an academic rig. The underlying theory regarding the GLRT-based indicator and the Rayleigh quotient optimization is laid out in Section 2. The proof of concept on simulated signals and the results of the performance tests on experimental signals are demonstrated in Section 3. The conclusive remarks and key findings are given in Section 4.

2 Methodology

The indicator used as the measure to be maximized is derived using the GLRT. Furthermore, the indicator is written in the generalized Rayleigh quotient form to optimize the filter. Therefore, a brief explanation of the GLRT and the generalized Rayleigh quotient is needed.

2.1 Generalized likelihood ratio test

The generalized likelihood ratio test is a member of the likelihood test family, hence, it compares how well a distribution fits one of the two proposed hypotheses. These hypotheses can be called H_1 and H_0 (null hypothesis). In essence these hypotheses represent the *damaged* and *healthy* state of the signal or the machine, respectively [9]. Signals to be tested are linked with the hypotheses by describing each with different probability functions (PDF). Thus, H_0 and H_1 can be defined as follows:

$$\begin{aligned} H_0 &: x(n) \sim p_x(\boldsymbol{x}|H_0, \boldsymbol{\theta_0}) \\ H_1 &: x(n) \sim p_x(\boldsymbol{x}|H_1, \boldsymbol{\theta_1}) \end{aligned} \tag{1}$$

where p_x represents the PDF parameterized by either $\boldsymbol{\theta_0}$ or $\boldsymbol{\theta_1}$ and $\boldsymbol{x}$ is the signal. The quantities in bold indicate that they are either vector or matrix quantities, and the amplitude of a signal at any time n is noted with $x(n)$. Then, the GLRT can be written as:

$$\Lambda(\boldsymbol{x}) = \frac{p_x(\boldsymbol{x}|H_1, \hat{\boldsymbol{\theta}}_{\boldsymbol{1}})}{p_x(\boldsymbol{x}|H_0, \hat{\boldsymbol{\theta}}_{\boldsymbol{0}})} \tag{2}$$

which already displays the form of the indicator. In Eq. 2, the quantities $\hat{\boldsymbol{\theta}}_{\boldsymbol{0}}$ and $\hat{\boldsymbol{\theta}}_{\boldsymbol{1}}$ are the maximum likelihood estimates (MLE) of the defined probability density functions. Therefore, if hypothesis one tends to hold for consecutive measurements, in other words, the MLE of the numerator in Eq. 2 is higher, then Λ would increase. If, on the other hand, H_1 does not hold, then the indicator converges to unity. A useful feature of the generalized likelihood ratio test is being equal to one or higher values. The GLRT is generally

expressed as a logarithm as it offers mathematical conveniences for the maximum likelihood estimations. Therefore, an indicator can be defined in the log-likelihood form as follows [9]:

$$ln(\Lambda(\boldsymbol{x})) = \sum_{n=0}^{L-1} ln(p_x(\boldsymbol{x}|H_1, \hat{\boldsymbol{\theta}}_{\mathbf{1}})) - \sum_{n=0}^{L-1} ln(p_x(\boldsymbol{x}|H_0, \hat{\boldsymbol{\theta}}_{\mathbf{0}})) \tag{3}$$

Hence, with $\mathcal{L}_{H_1}$ and $\mathcal{L}_{H_0}$ being the log-likelihoods of hypotheses H_1 and H_0, respectively, Eq. 3 can be rewritten as:

$$I_{H_1/H_0} = c\frac{\mathcal{L}_{H_1} - \mathcal{L}_{H_0}}{L} \geq 0 \tag{4}$$

Now that the indicator definition using the GLRT is briefly explained, the derivation of the indicator utilized in this study can be laid out.

2.1.1 Indicator derivation

One of the proposed indicators in [9] is defined to test non-Gaussianity versus Gaussianity of vibration signals under the stationary assumption. Therefore, the former defined via generalized Gaussian PDF is tested against the null hypothesis that assumes the latter. Hence, the hypotheses can be written as:

$$\begin{aligned} H_0 &: x \sim \mathcal{N}(\boldsymbol{x}; 0, \sigma) \\ H_1 &: x \sim G\mathcal{N}(\boldsymbol{x}; 0, \boldsymbol{\eta}, \beta) \end{aligned} \tag{5}$$

where σ, η, and β denote the variance, the scale parameter and the shape factor, respectively. Introducing the MLE of these hypotheses into Eq. 4 forms the indicator that tests non-Gaussianity versus Gaussanity [9], which is demonstrated as:

$$I_{GGS/GS}(\boldsymbol{x}) = ln\langle|x(n)|^2\rangle - \frac{2}{\hat{\beta}} ln\langle|x(n)|^{\hat{\beta}}\rangle + 2C(c, 2, \hat{\beta}) \tag{6}$$

In Eq. 6, the shape factor $\hat{\beta}$ is the MLE of the generalized Gaussian PDF and the function C can be found in Appendix B. For the details of the MLE of H_0 and H_1 readers can refer to [9]. In the original study, an approximate form of $I_{GGS/GS}$ is also proposed as [9]:

$$I'_{GGS/GS}(\boldsymbol{x}) = ln\left(\frac{\langle|x(n)|^2\rangle}{\langle|x(n)|^{\hat{\beta}}\rangle^{\frac{2}{\hat{\beta}}}}\right) \tag{7}$$

In the present study, the figure of merit to be maximized using Rayleigh quotient iteration is chosen to be the indicator $I'_{GGS/GS}$ as it is free from the mathematical complexity that comes along with the function C. This indicator essentially assesses the impulsiveness of the signal. The shape factor $\hat{\beta}$ is a measure of the deviation of the distribution from the Gaussian, and as β converges to zero, the distribution tends to be more impulsive. This indicator is further written in the Rayleigh quotient form to be maximized.

2.2 Rayleigh quotient derivation

The underlying idea is to filter the vibration signals with an optimal finite impulse response filter to maximize the measure of interest of the signal. Therefore, the indicator is formed based on the filtered signal $\boldsymbol{s}$, estimated with the following convolution of the raw signal $\boldsymbol{x}$ with length L.

$$\boldsymbol{s} = \boldsymbol{x} * \boldsymbol{h} \tag{8}$$

Let $\boldsymbol{h}$ be the filter; the convolution shown in Eq. 8 can be written in matrix form as follows:

$$\boldsymbol{s} = \boldsymbol{X}\boldsymbol{h} \tag{9}$$

where $\boldsymbol{X}$ is a 2D matrix version of $\boldsymbol{x}$. It must be noted that the filtered signal $\boldsymbol{s}$ is not expected to be the source signal, but it is an approximation at which the figure of merit is maximum. Hence, the filtered signal is plugged into the expression of $I'_{GGS/GS}$ defined in Eq. 6 and taking the exponential of both sides of the equation, the following expression is obtained.

$$\exp(I'_{GGS/GS}(\boldsymbol{x})) = \frac{\langle |s(n)|^2 \rangle}{\langle |s(n)|^{\hat{\beta}} \rangle^{\frac{2}{\hat{\beta}}}} \tag{10}$$

The indicator is defined in the exponential function to form the Rayleigh quotient. Since the exponential is a positive real-valued function, maximizing the $\exp(I'_{GGS/GS})$ is equivalent to maximizing the indicator with regard to the filter optimization. In other words, the filter optimized for the highest $\exp(I'_{GGS/GS})$ also results in the maximum of the $I'_{GGS/GS}$ of the filtered signal $\boldsymbol{s}$.

The numerator of the Eq. 10 can be expressed in matrix form as:

$$\langle |s(n)|^2 \rangle = \frac{1}{L}\boldsymbol{s}^H\boldsymbol{s} \tag{11}$$

The denominator, on the other hand, requires several more steps to write in the final form. For clarity, the derivation steps of the quantity at the denominator of Eq. 10 are given in Appendix C. The final form of the denominator, hence, is expressed as:

$$\langle |s(n)|^{\hat{\beta}} \rangle^{\frac{2}{\hat{\beta}}} = \boldsymbol{s}^H diag\left(\frac{|s(n)|^{\hat{\beta}-2}}{\gamma}\right)\boldsymbol{s} \tag{12}$$

where γ is given as follows:

$$\gamma = L^{\frac{2}{\hat{\beta}}}(\boldsymbol{s}^H diag(|s(n)|^{\hat{\beta}-2})\boldsymbol{s}) \tag{13}$$

The final form of the Rayleigh quotient of the exponential form of the indicator $I'_{GGS/GS}$ is obtained by plugging Eqs. 11 and 12 into the expression shown in Eq. 10 of the exponential indicator. Hence, the following equation is obtained:

$$\exp(I'_{GGS/GS}(\boldsymbol{x})) = \frac{1}{L}\frac{\boldsymbol{h}^H\boldsymbol{X}^H\boldsymbol{X}\boldsymbol{h}}{\boldsymbol{h}^H\boldsymbol{X}^H diag\left(\frac{|s(n)|^{\hat{\beta}-2}}{\gamma}\right)\boldsymbol{X}\boldsymbol{h}} \tag{14}$$

Equation 14 already reveals the Rayleigh quotient form [10]. The maximum value of the generalized Rayleigh quotient can be estimated by solving the following generalized eigenvalue problem,

$$\boldsymbol{R_{w1}}\boldsymbol{h} = \boldsymbol{R_{w2}}\boldsymbol{h}\boldsymbol{\lambda} \tag{15}$$

where $\boldsymbol{R_{w1}}$ and $\boldsymbol{R_{w2}}$ are defined as

$$\boldsymbol{R_{w1}} = \boldsymbol{X}^H\boldsymbol{X} \tag{16}$$

$$\boldsymbol{R_{w2}} = \boldsymbol{X}^H diag\left(L\frac{|s(n)|^{\hat{\beta}-2}}{\gamma}\right)\boldsymbol{X} \tag{17}$$

The maximum eigenvalue and corresponding eigenvector are equivalent to the maximum value $\exp(I'_{GGS/GS}(\boldsymbol{x}))$ and the optimal filter, respectively. As mentioned, the exponential of the indicator is exploited to form the Rayleigh quotient. Nonetheless, the indicator $I'_{GGS/GS}$ is estimated over the signals filtered with the optimal filter. Hence, the results are shown and discussed based on $I'_{GGS/GS}$. Ideally, the optimal filter is expected to band-pass filter around the carrier frequency of the bearing fault; hence, the impulsive pattern caused by the bearing fault protrudes from noise.

2.2.1 Rayleigh quotient iteration

The generalized eigenvalue problem shown in Eq. 15 is solved via an iterative approach. A filter is initialized first to estimate $\boldsymbol{R_{w1}}$ and $\boldsymbol{R_{w2}}$ which are further used to solve for the eigenvalue and corresponding eigenvector. The maximum eigenvalue is accepted as the solution of the iteration step and is utilized in the next iteration. The solution is assumed to be converged when the relative error estimated based on the difference between two consecutive eigenvalues drops below $1\,\%$. The Rayleigh quotient iteration benefits from its rapid convergence rate as long as the numerical stability is satisfied [11]. A study on the effect of the filter parameters on the Rayleigh quotient iteration demonstrates that filter initialization does not significantly influence the solution while its length is problem-dependent [12]. Therefore, in this study, filters are initialized with the simple difference filter. It is basically an array of zeros where the second and the fourth point are 1 and -1, respectively. Moreover, filter lengths of 100 and 200 are chosen for the simulated and the experimental signals, as they provide the most conclusive results.

3 Results

This section demonstrates and discusses results from the simulated and the experimental vibration signals with roller element bearing faults.

3.1 Signal simulations

The proposed concept is first tried out on simulated vibration signals. Signals simulating vibrations emitted from a roller bearing with an outer race fault are generated with periodic impulses recurring at 20 Hz. These signals are convolved with an impulse response function with the carrier frequency of 1000 Hz. The slippage phenomenon is taken into account, and a deviation of no more than 2% of the fault frequency is introduced to the impulses. White noise is added to vary the signal-to-noise (SNR) from -30 dB to 30 dB.

Figure 1 demonstrates the evolution of the $I'_{GGS/GS}$ estimated over the filtered and the raw signals. The indicator level persists near zero for both the raw and the filtered signals up to the SNR of around -8.5 dB, after which a sharp increase in the trend of the filtered signal is observed. The peak point of this first increase is around 30 times the initial value. On the other hand, the trend of $I'_{GGS/GS}$ of the raw signals smoothly rises and reaches the same level as the peak of the initial increase of the filtered signals at around SNR of 1 dB. The early increase in the trend of the filtered signals compared to the raw signals implies that the Rayleigh quotient optimization succeeds in estimating an optimal filter to maximize $I'_{GGS/GS}$ and the impulsive pattern purports from the noisy signal. Further trends of $I'_{GGS/GS}$ for the raw and the filtered signals exhibit similar behaviour where the value of the indicator for both trends is increasing. However, it must be noted that the indicator level for the filtered signals is always approximately 1.5 to 2 times higher than the raw signals. Furthermore, at considerably high SNR, while the trend $I'_{GGS/GS}$ of the raw signals exhibits a converging behaviour, that of the filtered signals demonstrates an ever-increasing pattern. This nuance may be crucial to accurately assess the severity of a bearing fault if such high SNR levels are attained.

The efficacy of the filtering, which results in a higher value of the indicator on filtered signals, is further scrutinized. Therefore, the first 2000 samples of the raw and the filtered signal at -7 dB, which corresponds to the position of the dashed line in Fig. 1, are displayed in Fig. 2 in the time domain and inspected. The impulsive pattern is recovered on the filtered signal which inherently results in a more significant level

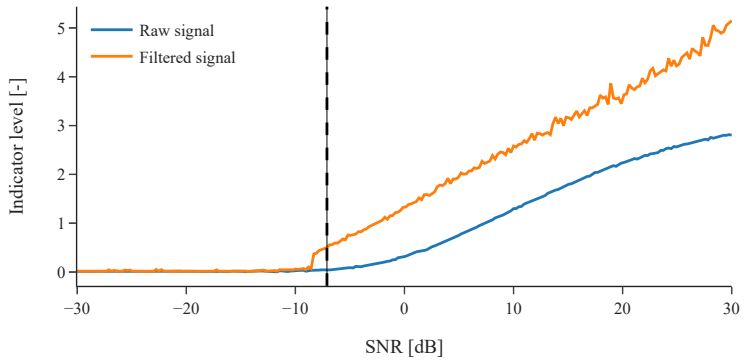

Figure 1: Evolution of the indicator for the filtered and the raw simulated signals

of $I'_{GGS/GS}$ on the filtered signal than the raw signal. Moreover, as the distributions of these signals are considered, Fig. 3 illustrates the higher occurrence at the tails of the amplitude distribution for the filtered signal. In other words, the amplitude distribution of the filtered signal deviated from the Gaussian distribution which causes the increase of $I'_{GGS/GS}$.

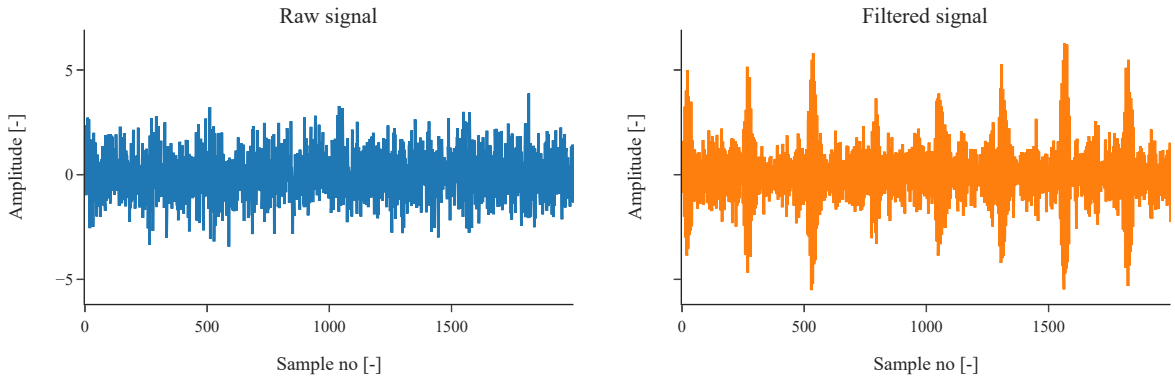

Figure 2: The raw and the filtered signals at -7 dB SNR

The spectra of the filtered and the raw signals are also investigated to comprehend why the optimal filter recovers the impulsive pattern. The spectra of the two signals at -7 dB are shown in Fig. 4. The amplitudes of the frequency bins at around the carrier frequency of 1000 Hz are slightly higher than the noise floor on the spectrum of the raw signal. On the other hand, it can be deduced from the spectrum of the filtered signal that the carrier frequency is band-pass filtered. The amplitude of the noise floor is reduced while the amplitudes around 1000 Hz are increased due to filtering. This also stresses that the optimal filter performs as intended such that it promotes impulsiveness by band-pass filtering the carrier frequency of the simulated vibration signals with a bearing faults.

An important issue regarding the Rayleigh quotient iteration is its numerical stability. Numerical stability and convergence behaviour may be of concern for relatively long filters. The relative error trends of the Rayleigh quotient iteration for simulated signals at six different SNR levels are displayed in Fig. 5. Iterations made for the low SNR signals reach the threshold at the first iteration, while for larger SNR signals, the threshold is met at higher iterations. The critical point concerning the numerical stability is the monotonous decline of the relative error down to the threshold value. This smooth decrease is observed for all simulated signals. A representative subset of six trends are shown in Fig. 5 for clarity.

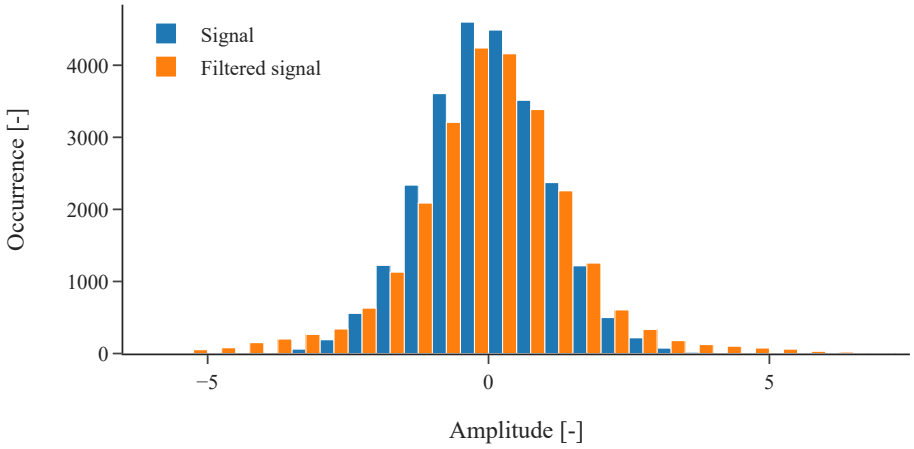

Figure 3: Histogram of the raw and the filtered signals at −7 dB SNR

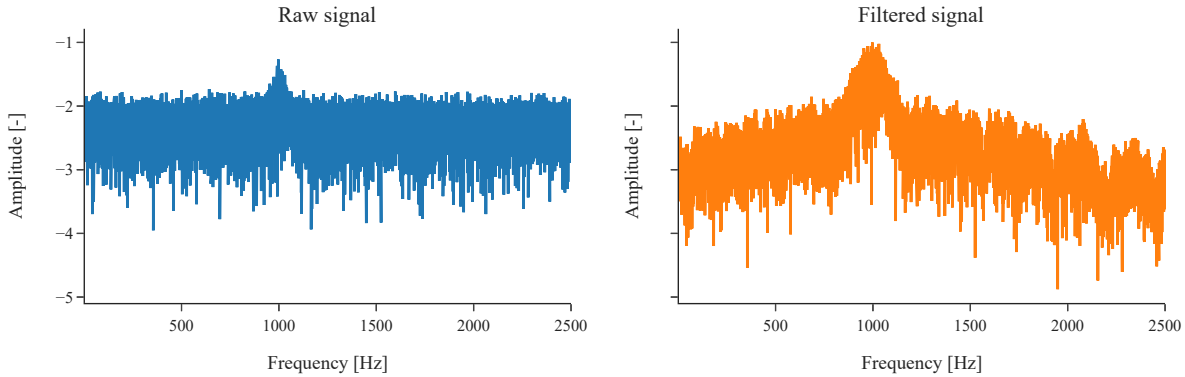

Figure 4: Spectra of the raw and the filtered signals at −7 dB SNR

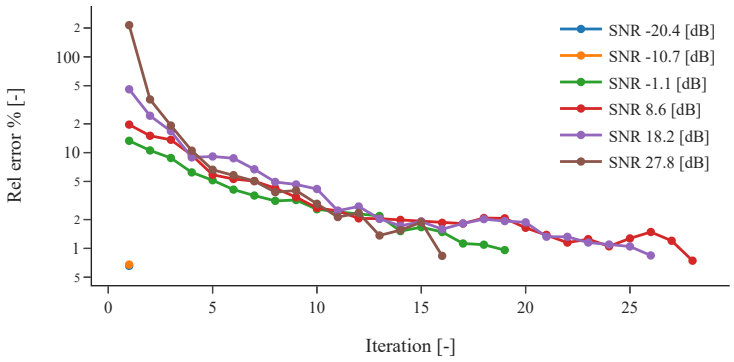

Figure 5: The trends of relative error during the Rayleigh quotient iterations for several simulated signals

3.2 Experimental signals

The vibration signals are measured on an academic test rig, and the dataset is made available by Flanders Make. The three datasets utilized in this study are sampled for one second or ten seconds at 50 kHz rate. The measurements are run-to-failure tests initiated with Rockwell-C indentation of 100 kg in the bearing inner

race of the bearing 6205-C-TVH. Measurements are performed at constant speeds of 2000 rpm and 1800 rpm for one-second and ten-second signals, respectively. The vibration sensors are located in the vicinity of the bearings; hence the only considerable source of vibration is the bearing fault. Therefore, signals do not need to be whitened. The measurements are named as dataset 1, 2, and 3. While the first two datasets are comprised of one-second long signals, the third dataset is sampled for 10 seconds.

The indicator trends estimated over the filtered and raw signals of dataset 1 are shown in Fig. 6a. The initial level of $I'_{GGS/GS}$ for the *healthy* state of the signal is near zero and steady for both signals. Then an initial increase is observed on both the filtered and the raw signal trends at around measurement 160, after which they demonstrate a similar trend. The level of the indicator, however, for the filtered signals is much higher than the raw signal, which may allow the end-user to be alarmed regarding the presence of an anomaly in a more robust manner. The visual inspection of the raw and filtered signals explains the difference since the impulses of the filtered signals are more dominant compared to the raw signals, as can be seen in Fig. 6b.

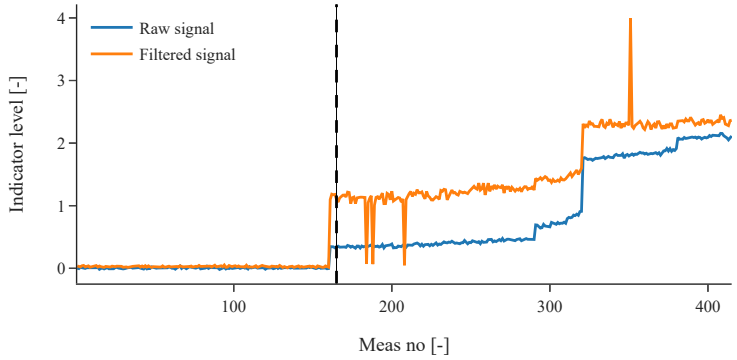

(a) Evolution of the indicator estimated on filtered and raw signals

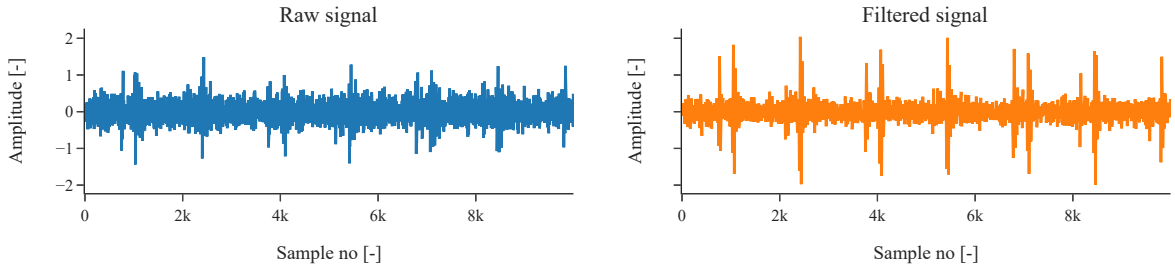

(b) The raw and the filtered signals of the measurement shown with the dashed line

Figure 6: Results obtained on dataset 1

A scenario similar to dataset 1, where the initial plateau representing the *healthy* phase of the signal is followed by a sharp rise on the indicator for both raw and filtered signals, is observed in Fig. 7a for dataset 2. Detail must be noted that on the trend of the filtered signals, the initial increase is followed by a falling and rising pattern of 3 measurements where the drop reaches the level of $I'_{GGS/GS}$ of the raw signals. This occurs because the iterative solution fails to find the optimal filter; hence, the filtered signal is not significantly different from the original signal. Another interesting detail appears after around measurement 388. There is a descending trend starting at around measurement 388 on the indicator level of the raw signals. This could be because the fault tends to become distributed; thus, the signal distribution tends to be less impulsive. On the other hand, the increasing trend persists for the filtered signals after measurement 388 because the optimized filter is capable of maximizing the impulsiveness of the signals. The stronger impulsive pattern can also be observed on filtered signals compared to the raw signal in the time domain in Fig. 7b.

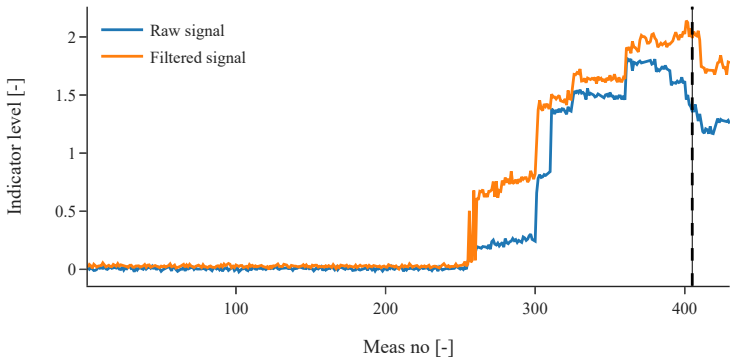

(a) Evolution of the indicator estimated on filtered and raw signals

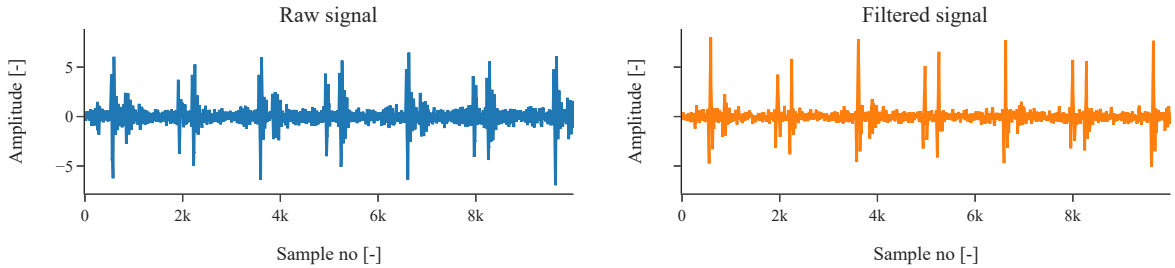

(b) The raw and the filtered signals of the measurement shown with the dashed line

Figure 7: Results obtained on dataset 2

The third dataset, as mentioned above, is comprised of ten-seconds signals. The level of $I'_{GGS/GS}$ for the filtered signals is almost twice that of the raw signals for the *damaged* state of the signals. It must be noted that the trends are smoother than in the previous two graphs. This is because the MLE is performed more accurately as signals are longer. Moreover, the filter may be optimized in a more accurate manner as the frequency resolution of a ten-second signal is higher than a one-second signal. Therefore, the trends of the lines in Fig. 8a are free from abrupt drops and rises. The clear difference between the filtered and the raw signals is demonstrated in Fig. 8b. The filtered signal at the measurement shown with the dashed line on Fig. 8a demonstrates evident peaks with higher amplitudes than the peaks in the raw signal in the time domain.

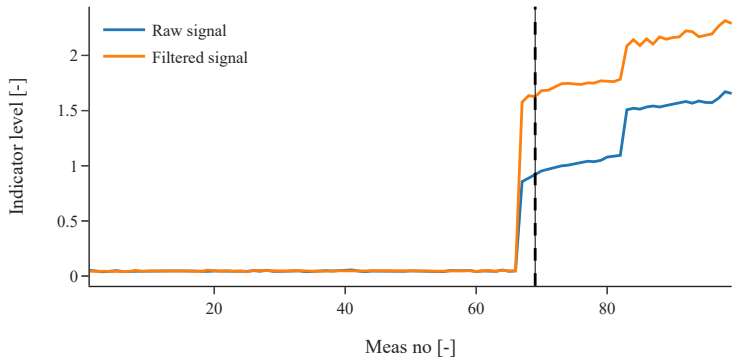

(a) Evolution of the indicator estimated on filtered and raw signals

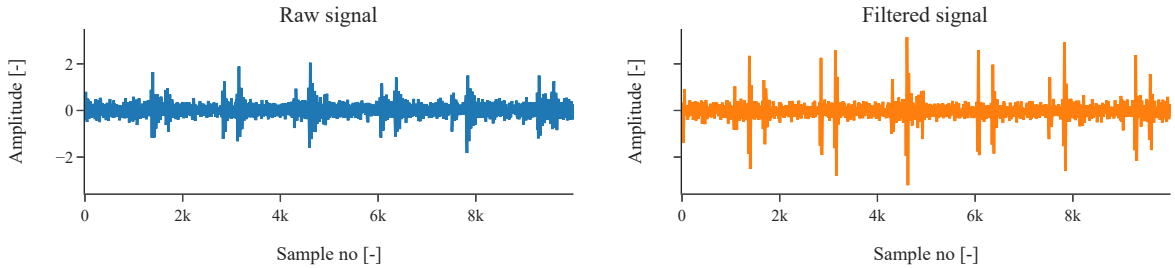

(b) The raw and the filtered signals of the measurement shown with the dashed line

Figure 8: Results obtained on dataset 3

4 Conclusion

This study aims to investigate the capability of blind filtering to enhance the fault detection performance of a Generalized Likelihood Ratio Test-based indicator. It is demonstrated that the indicator, $I'_{GGS/GS}$, developed using the GLRT can be written in the generalized Rayleigh quotient form. Furthermore, the optimal blind filter can be evaluated via Rayleigh quotient optimization to maximize the indicator estimated on the filtered signals. The approach is first tried out on simulated signals for the proof of concept. The outcome stresses that the method has the potential for the early and robust detection of roller element bearing faults. The onset of the increasing trend of the GLRT-based indicator estimated on filtered signals is observed significantly earlier than that of the raw signals. Moreover, the indicator level is considerably higher in filtered signals, which allows for developing more robust alarming for the end-user. The results obtained from the experimental signals also partly confirm the outcomes of the signal simulations. The rise of $I'_{GGS/GS}$ appears to be higher from the *healthy* to the *damaged* state of the machine on filtered signals. Hence, it offers a more reliable alarm for bearing fault detection purposes. On the other hand, an early onset for the rising trend is not achieved for the filtered signals. A significant aspect of the proposed method is that it requires no input regarding the machine kinematics. However, it can only offer anomaly detection but cannot be directly employed for diagnostic purposes since the fault detection is performed based on the deviation of the signal distribution from the Gaussian, which may be caused due to interference from several components in a rotating machine. This approach can be extended to further vibration-based indicators for early and robust detection of anomalies in rotating machinery.

Acknowledgements

This research received funding from the Flemish Government under the “Onderzoeksprogramma Artificiële Intelligentie (AI) Vlaanderen” program. The authors would like to acknowledge FWO (Fonds Wetenschappelijk Onderzoek) for their support through the post-doctoral grant of Cedric Peeters (1282221N) and SBO

project Robustify (S006119N). The authors also would like to acknowledge the support of Blue Cluster ICON project Supersized 4.0.

References

[1] R. A. Wiggins, "Minimum entropy deconvolution," *Geoexploration*, vol. 16, no. 1-2, pp. 21–35, 1978.

[2] W. C. Gray, "Variable norm deconvolution," Ph.D. dissertation, Stanford University Ph. D. thesis, 1979.

[3] G. L. McDonald, Q. Zhao, and M. J. Zuo, "Maximum correlated kurtosis deconvolution and application on gear tooth chip fault detection," *Mechanical Systems and Signal Processing*, vol. 33, pp. 237–255, nov 2012.

[4] J. Obuchowski, R. Zimroz, and A. Wyłomańska, "Blind equalization using combined skewness–kurtosis criterion for gearbox vibration enhancement," *Measurement*, vol. 88, pp. 34–44, jun 2016.

[5] X. Jiang, X. Cheng, J. Shi, W. Huang, C. Shen, and Z. Zhu, "A new l0-norm embedded MED method for roller element bearing fault diagnosis at early stage of damage," *Measurement*, vol. 127, pp. 414–424, oct 2018.

[6] M. Buzzoni, J. Antoni, and G. D'Elia, "Blind deconvolution based on cyclostationarity maximization and its application to fault identification," *Journal of Sound and Vibration*, vol. 432, pp. 569–601, oct 2018.

[7] C. Peeters, J. Antoni, and J. Helsen, "Blind filters based on envelope spectrum sparsity indicators for bearing and gear vibration-based condition monitoring," *Mechanical Systems and Signal Processing*, vol. 138, p. 106556, apr 2020.

[8] C. López, D. Wang, Á. Naranjo, and K. J. Moore, "Box-cox-sparse-measures-based blind filtering: Understanding the difference between the maximum kurtosis deconvolution and the minimum entropy deconvolution," *Mechanical Systems and Signal Processing*, vol. 165, p. 108376, feb 2022.

[9] P. B. J. Antoni, "A statistical methodology for the design of condition indicators," *Mechanical Systems and Signal Processing*, vol. 114, pp. 290–327, jan 2019.

[10] R. A. Horn and R. Johnson, Eds., *Matrix Analysis*. Cambridge University Press, 1985.

[11] B. N. Parlett, "The rayleigh quotient iteration and some generalizations for nonnormal matrices," *Mathematics of Computation*, vol. 28, no. 127, pp. 679–693, 1974.

[12] K. Kestel, C. Peeters, J. Antoni, and J. Helsen, "Fault detection via sparsity-based blind filtering on experimental vibration signals," *Annual Conference of the PHM Society*, vol. 13, no. 1, nov 2021.

Appendix

A Nomenclature

A	Cross-sectional area
CI	Condition indicator
GS	Gaussian stationary
GGS	Generalized Gaussian stationary
$GLRT$	Generalized likelihood ratio test
MED	Minimum entropy deconvolution
$MCKD$	Maximum correlated kurtosis deconvolution
MLE	Maximum likelihood estimation
PDF	Probability density function
SNR	Signal-to-noise ratio

B Auxillary functions

The explicit form of the quantity C given in Eq. 10 [9].

$$C(c,\hat{\beta}_0,\hat{\beta}_1) = ln\left(\frac{\hat{\beta}_0^{\frac{1}{\hat{\beta}_0}-1}\Gamma(c/\hat{\beta}_0)}{\hat{\beta}_1^{\frac{1}{\hat{\beta}_1}-1}\Gamma(c/\hat{\beta}_1)}\right) + \frac{1}{\hat{\beta}_0} - \frac{1}{\hat{\beta}_1} \tag{18}$$

C Rayleigh quotient derivation details

The denominator of Eq. 10 can be written as follows:

$$\langle|s(n)|^{\hat{\beta}}\rangle^{\frac{2}{\hat{\beta}}} = \left\langle\frac{|s(n)|^2}{|s(n)|^{2-\hat{\beta}}}\right\rangle^{2/\hat{\beta}} \tag{19}$$

Re-writing it in matrix form results in the following:

$$\langle|s(n)|^{\hat{\beta}}\rangle^{\frac{2}{\hat{\beta}}} = \left(\frac{1}{L}\boldsymbol{s}^H diag\left(\frac{1}{|s(n)|^{2-\hat{\beta}}}\right)\boldsymbol{s}\right)^{2/\hat{\beta}} \tag{20}$$

Both numerator and denominator of Eq. 20 is multiplied by $\boldsymbol{s}^H\boldsymbol{s}$ to obtain the following form.

$$\langle|s(n)|^{\hat{\beta}}\rangle^{\frac{2}{\hat{\beta}}} = \frac{1}{L^{\hat{\beta}/2}}\frac{\boldsymbol{s}^H diag(|s(n)|^{\hat{\beta}-2})\boldsymbol{s}}{(\boldsymbol{s}^H diag(|s(n)|^{\hat{\beta}-2})\boldsymbol{s})^{1-2/\hat{\beta}}} \tag{21}$$

Now that the $\boldsymbol{s}^H$ and $\boldsymbol{s}$ appears in the left and the right hand side of Eq. 21, respectively, the following expression can be used to form the denominator of the Rayleigh quotient.

$$\langle|s(n)|^{\hat{\beta}}\rangle^{\frac{2}{\hat{\beta}}} = \boldsymbol{s}^H diag\left(\frac{1}{L^{\hat{\beta}/2}}\frac{diag(|s(n)|^{\hat{\beta}-2})}{(\boldsymbol{s}^H diag(|s(n)|^{\hat{\beta}-2})\boldsymbol{s})^{1-2/\hat{\beta}}}\right)\boldsymbol{s} \tag{22}$$

The expression γ is defined as follows to simplify the final equation.

$$\gamma = L^{2/\hat{\beta}}(\boldsymbol{s}^H diag(|s(n)|^{\hat{\beta}-2})\boldsymbol{s})^{1-2/\hat{\beta}} \tag{23}$$